Non-Hermitian topological excitation transmission in the dimerized lattice with imaginary potential and nonreciprocal hopping

Lu Qi,[1,*] Qiao-Nan Li,[1] Ning Han,[2] Mingzhu Li,[3,†] Xiu-Yun Zhang,[1] and Ai-Lei He[1,‡]
[1]*School of Physical Science and Technology, Yangzhou University, Yangzhou 225002, China*
[2]*Interdisciplinary Center for Quantum Information, State Key Laboratory of Modern Optical Instrumentation, College of Information Science and Electronic Engineering, Zhejiang University, Hangzhou 310027, China*
[3]*School of Information and Electrical Engineering, Hangzhou City University, Hangzhou 310015, China*

(Received 7 November 2023; revised 12 January 2024; accepted 8 March 2024; published 25 March 2024)

We investigate the topological edge transmission of excitation based on the one-dimensional Su-Schrieffer-Heeger lattice with purely imaginary on-site potential and nonreciprocal nearest-neighbor hopping. We find that, when the system has only the nonreciprocal intracell hopping, the topological excitation transmission can be implemented only when the localization direction of the non-Hermitian skin effect matches the localization direction of edge state. When the lattice has the purely imaginary on-site potential and nonreciprocal intracell hopping, we demonstrate that the positive purely imaginary potential is the dominant effect of implementing the topological excitation transmission compared with the non-Hermitian skin effect. Furthermore, we also investigate the joint effect between the purely imaginary on-site potential and nonreciprocal intercell hopping, which reveals that the non-Hermitian skin effect induced via the large nonreciprocal parameter determines the successful topological excitation transmission. Our investigations show the different influences of two kinds of non-Hermitian effects on the topological excitation transmission, which may promote the implementation of topological transmission in the practical open quantum system.

DOI: 10.1103/PhysRevA.109.032428

I. INTRODUCTION

Quantum information processing, with information encoding on the quantum states, has attracted increasing attention in recent years [1–6]. Benefitting from the superposition and entanglement properties of quantum states, quantum information processing presents a unique advantage in terms of efficiency and security compared with classical information processing [2,3,6–15]. One fundamental and critical step in quantum information processing is how to implement the efficient transmission of a quantum state between remote nodes without the influence of channel noise [16–25]. To this end, various kinds of schemes have been developed to realize robust quantum state transfer, including photon pulse shaping [26–28], adiabatic state transfer [20,23,24,29,30], Hamiltonian engineering [31–33], quantum error correction [34–36], and even topological quantum state transfer [37–42].

Topological quantum state transfer, implementing the quantum transmission via the boundary state of the topological insulator, can effectively resist the effects of local disorder in the channel [43–47]. The robustness of topological state transfer against disorder essentially originates from the topological protection of the band gap; i.e., the gap state remains unchanged until the gap is closed [44–47]. For example, in Ref. [48], a scheme of robust quantum state transfer was proposed in a dipolar array, in which quantum state transfer thorough the chiral edge states is robust against dispersive and disorder effects. Subsequently, the efficient exchange of quantum information over large distances in a linear network of coupled bosonic degrees of freedom was implemented [49]. In addition, robust quantum state transfer schemes were also proposed in the superconducting circuit [50], waveguide array [51], optomechanical array [52], elastic lattices [53], and acoustic system [54]. Topological quantum state transfer schemes usually focus on the transmission of the quantum state from one node to another node and are time-consuming due to the adiabatic evolution, which has prompted investigations of scalable topological distributions [55–59] and accelerated topological transmissions [60–63].

Note that the above works on topological quantum state transfer mainly considered the Hermitian assumption in which non-Hermitian effects are rarely involved. Recently, the topological band theory was extended to the non-Hermitian versions of the topological insulator, revealing abundant topological phenomena, e.g., the typical spontaneous breaking of parity-time symmetry induced by the opposite purely imaginary on-site potential [64–70]. For the negative purely imaginary on-site potential, it can be regarded as dissipation in the quantum system, which usually has adverse effects on quantum state transfer. And the breaking of parity-time symmetry, leading to the appearance of the imaginary part of the eigenvalues, also may affect the dynamical evolution of the quantum state [71,72]. In addition to the non-Hermitian topological system induced by the imaginary potential, the non-Hermitian skin effect and non-Bloch theory in the

*luqi@yzu.edu.cn
†limz@zucc.edu.cn
‡heailei@yzu.edu.cn

topological system with nonreciprocal hopping have also attracted a great deal of attention in recent years [73–78]. Different from the traditional Bloch bulk states with extended distributions, the non-Hermitian skin effect causes all of the bulk states to be localized around one boundary [78]. The localized bulk states usually correspond to the directional transmission [79,80], which may have a great influence on the topological edge transmission of quantum state. Thus, it is interesting to investigate the effects of these non-Hermitian topological phenomena on the topological edge transmission, especially the simultaneous impacts of the breaking of parity-time symmetry and the non-Hermitian skin effect on the topological edge transmission.

In this paper, we investigate the topological edge transmission of excitation in a non-Hermitian Su-Schrieffer-Heeger (SSH) lattice with purely imaginary on-site potential and nonreciprocal nearest-neighbor (NN) hopping. We find that, when the system has only nonreciprocal intracell hopping, the localized directions of the gap state and skin effect determine the opening of the topological excitation transmission. Namely, only when the localized direction of the gap state remains consistent with the non-Hermitian skin effect of bulk states can the excitation initially prepared at the left edge be transmitted to the right edge. When the system has nonreciprocal intracell hopping and a purely imaginary on-site potential simultaneously, we find that the purely imaginary on-site potential is the key factor to determine the opening of the topological excitation transmission, in which the excitation can be transmitted to the right edge successfully as long as the amplitude of the purely imaginary on-site potential keeps positive. Furthermore, we also discuss the effects of nonreciprocal intercell hopping and purely imaginary on-site potential on the topological excitation transmission. We find that the large nonreciprocal parameter of intercell hopping can promote the topological excitation transmission in the case of both vanishing and nonvanishing purely imaginary on-site potential. Our investigations further reveal the effects of non-Hermitian terms on the topological excitation transmission and show the interplay between the purely imaginary on-site potential and nonreciprocal hopping.

This paper is organized as follows: In Sec. II, we show the different effects of the purely imaginary on-site potential and nonreciprocal hopping and their joint effect on the topological excitation transmission. A conclusion is given in Sec. III.

II. NON-HERMITIAN TOPOLOGICAL EXCITATION TRANSMISSIONS IN THE LATTICE WITH AN IMAGINARY POTENTIAL AND NONRECIPROCAL HOPPING

A. Model and Hamiltonian

We consider the SSH chain containing the purely imaginary on-site potential and nonreciprocal coupling simultaneously, as shown in Fig. 1. We show two different kinds of configurations of nonreciprocal hopping, i.e., the nonreciprocal intracell hopping shown in Fig. 1(a) and the nonreciprocal intercell hopping shown in Fig. 1(b). Note that the SSH chain has an odd-size lattice $L = 2N + 1$ ($N \in$ even), in which the green (red) sites denote the negative (positive) purely

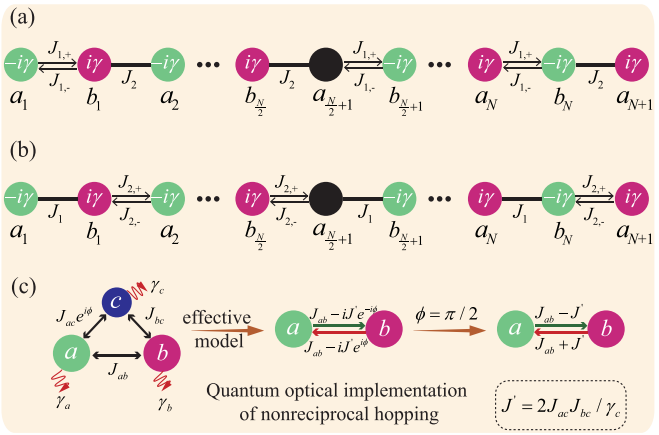

FIG. 1. The diagrammatic sketch of the non-Hermitian SSH model. (a) The non-Hermitian SSH model has nonreciprocal intracell hopping and purely imaginary on-site potential. (b) The non-Hermitian SSH model has nonreciprocal intercell hopping and purely imaginary on-site potential. (c) The implementation of the nonreciprocal hopping in a three-mode system.

imaginary potentials and the central black site represents the vanishing imaginary potential. For convenience, we consider the SSH chain with the nonreciprocal intracell hopping (which we denote model 1) first [see Fig. 1(a)]; it can be described by the following Hamiltonian:

$$\begin{aligned} H = & \sum_{n=1}^{N/2}(-i\gamma a_n^\dagger a_n + i\gamma b_n^\dagger b_n) \\ & + \sum_{n=N/2+1}^{N}(-i\gamma b_n^\dagger b_n + i\gamma a_{n+1}^\dagger a_{n+1}) \\ & + \sum_{n=1}^{N}[J_{1,-}a_n^\dagger b_n + J_{1,+}b_n^\dagger a_n \\ & + J_2(a_{n+1}^\dagger b_n + \text{H.c.})]. \end{aligned} \tag{1}$$

Here, a_n ($a_n^\dagger$) and b_n ($b_n^\dagger$) denote the annihilation (creation) operators of the lattice chain, $-i\gamma$ and $i\gamma$ represent the purely imaginary on-site potentials, $J_{1,\pm}$ is the amplitude of the nonreciprocal intracell hopping, and J_2 is the amplitude of the reciprocal intercell hopping. To implement the topological excitation transmission, we set the intracell (intercell) hopping amplitudes as $J_{1,\pm} = J \pm \delta\cos\theta$ ($J_2 = J + \cos\theta$) and set $J = 1$ as the energy unit. Note that the parameter δ in the hopping amplitude is the nonreciprocal coefficient and $\theta \in [0, 2\pi]$ is the periodic parameter. The quantum optical implementation of the nonreciprocal hopping is shown in Fig. 1(c), in which two modes, a and b, are coupled directly via J_{ab} and indirectly via the assisted mode c. Under the dissipative regime, the assisted mode c can be effectively eliminated, causing the effective coupling between modes a and b to be asymmetric (see Appendix A). When $\gamma = 0$ and $\delta = 0$, the present model becomes a standard odd-sized SSH chain, which has a topologically nontrivial zero-energy gap state implementing the topological excitation transfer [50]. Then,

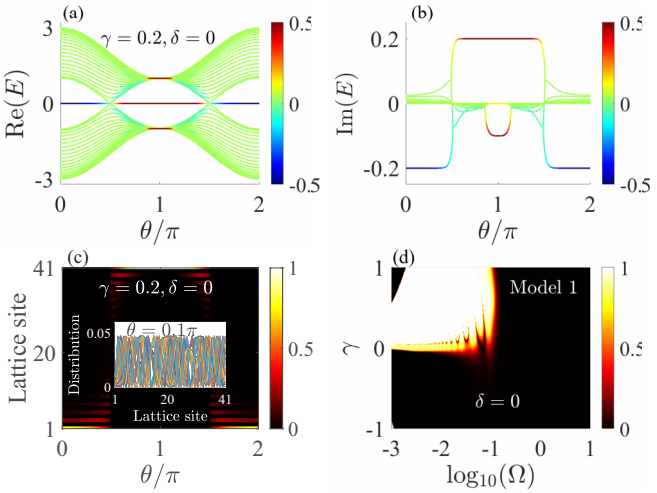

FIG. 2. Energy spectra, distributions of states, and fidelity for model 1 when $\delta = 0$. (a) The real and (b) imaginary parts of the energy spectra when $\gamma = 0.2$ and $\delta = 0$. The colored lines represent the dIPR of states. (c) The distributions of gap and bulk states. The inset shows the distributions of bulk states when $\theta = 0.1\pi$. (d) The fidelity of the topological excitation transmission versus varying speed Ω and amplitude of the imaginary potential γ.

how do the imaginary potential and the nonreciprocal hopping affect the topological excitation transmission?

B. Topological excitation transmission enhanced via the imaginary potential

We first recall the case of $\delta = 0$ and $\gamma \neq 0$ [72]. The real and imaginary parts of the energy spectrum are shown in Figs. 2(a) and 2(b), in which the colored levels represent the corresponding directional inverse participation ratio (dIPR) of the eigenstates. The dIPR of one (kth) eigenstate can be defined as $R_{\mathrm{dIP}}(\Psi_k) = \mathcal{P}(\Psi_k)\sum_j |\Psi_{n,j}|^4/(\langle\Psi_k|\Psi_k\rangle)$, which reveals the localization and localization direction of one eigenstate [81]. Here, $\mathcal{P}(\Psi_k) = \mathrm{sgn}[\sum_j (j - L/2 - \xi)|\Psi_k|^2]$ ($0 < \xi < 0.5$) means taking the sign of the argument. In this way, when the eigenstate is mainly localized at the left edge, we have $R_{\mathrm{dIP}} < 0$, while we have $R_{\mathrm{dIP}} > 0$ for the right-localized eigenstate. Especially, if one eigenstate is extended, the dIPR satisfies $R_{\mathrm{dIP}} \sim 0$. Obviously, when $\gamma = 0.2$ and $\delta = 0$, the bulk states of the system are extended, and the gap state is localized around the left (right) edge when $\theta \in [0, 0.5\pi] \cup [1.5\pi, 2\pi]$ [$\theta \in (0.5\pi, 1.5\pi)$]. To further verify this, we can plot the probability distribution $||\Psi_g\rangle|^2$ of the gap state $|\Psi_g\rangle$ versus the parameter θ and lattice site by solving the eigenenergy equation $H|\Psi_g(\theta)\rangle = E_g|\Psi_g(\theta)\rangle$, where E_g is the corresponding eigenenergy with a purely imaginary value (e.g., $E_g = -0.2i$ within $\theta \in [0, 0.5\pi]$ in Fig. 2(b)). The distribution of the gap state $|\Psi_g\rangle$ versus the parameter θ is plotted in Fig. 2(c). The results clearly reveal that the gap state is mainly localized at different edges within different ranges of the parameter θ. Furthermore, we also plot the distributions of all bulk states when $\theta = 0.1\pi$ in the inset of Fig. 2(c), and we find that all of the bulk states are, indeed, the extended states.

The gap state in the Hermitian SSH model can be used to implement the topological excitation transmission between two edge nodes. To implement the topological excitation transmission, the initial state needs to be evolved under the Schrödinger equation $i\frac{\partial}{\partial t}|\Psi\rangle = H(\theta_t)|\Psi\rangle$ after rewriting the parameter θ as the time-dependent version $\theta = \Omega t$ (Ω is a varying rate and t is time). If the excitation is prepared at the left edge initially, it will be evolved along the gap state and finally transmitted to the right edge. The transmission efficiency of the excitation can be estimated via the fidelity $F = |\langle R|\Psi_f\rangle|$ defined by the ideal right edge state $|R\rangle = |0, 0, \ldots, 0, 1\rangle$ and evolved final state $|\Psi_f\rangle$. Following this concept, the fidelity versus the varying rate Ω and amplitude of the pure potential γ is plotted in Fig. 2(d). The results reveal that the excitation transmission can be implemented only when $\gamma > 0$, which is consistent with the results in Ref. [72]. Note that the difference is that the gap state in this paper cannot be localized at the left edge completely, e.g., when $\theta = 0$. This means that the excitation initially prepared at the left edge actually cannot match the gap state (when $\theta = 0$) precisely. We stress that the excitation can still be transmitted to the right edge even though the initial state cannot match the gap state, which is rarely mentioned in previous works. Furthermore, different from the topological excitation transmission in the standard SSH lattice, the present non-Hermitian topological excitation transmission may not evolve along the gap state, implying a possible nonadiabatic transmission (see Appendix B).

C. Non-Hermitian skin effect and topological excitation transmission

We now focus on the case of $\gamma = 0$ and $\delta \neq 0$. Different from the case of $\gamma \neq 0$ and $\delta = 0$, the asymmetric intracell hopping can induce the non-Hermitian skin effect; i.e., all of the bulk states are mainly localized around one edge of the system. The energy spectrum and dIPR are plotted in Figs. 3(a) and 3(b). We find that the present non-Hermitian system corresponds to a purely real spectrum (see Appendix C). Especially, the bulk states of the present system exhibit the non-Hermitian skin effect; i.e., the bulk states are localized around the right (left) edge when $\theta \in [0, 0.5\pi] \cup [1.5\pi, 2\pi]$ [$\theta \in (0.5\pi, 1.5\pi)$]. Note that the direction of the localization of the bulk states is just the opposite of that of the gap state. The distributions of the gap state and bulk states are shown in Fig. 3(c), which shows results consistent with the above analysis. The non-Hermitian skin effect can usually affect the transmission properties, e.g., the directional transmission. To further estimate the effects of the non-Hermitian skin effect on the topological excitation transmission, the transmission fidelity versus the varying rate and the nonreciprocal parameter δ is plotted in Fig. 3(d).

The results indicate that only when $\delta < 0$ can the topological excitation transmission be implemented successfully. Detailed evolutions of the topological excitation transmission when $\delta = 0.5$ and $\delta = -0.5$ are shown in Figs. 3(e) and 3(f). Obviously, the excitation initially prepared at the left edge can be transmitted to the right edge only when $\delta < 0$. This phenomenon is quite counterintuitive since the right non-Hermitian skin effect ($\delta > 0$) usually leads to the

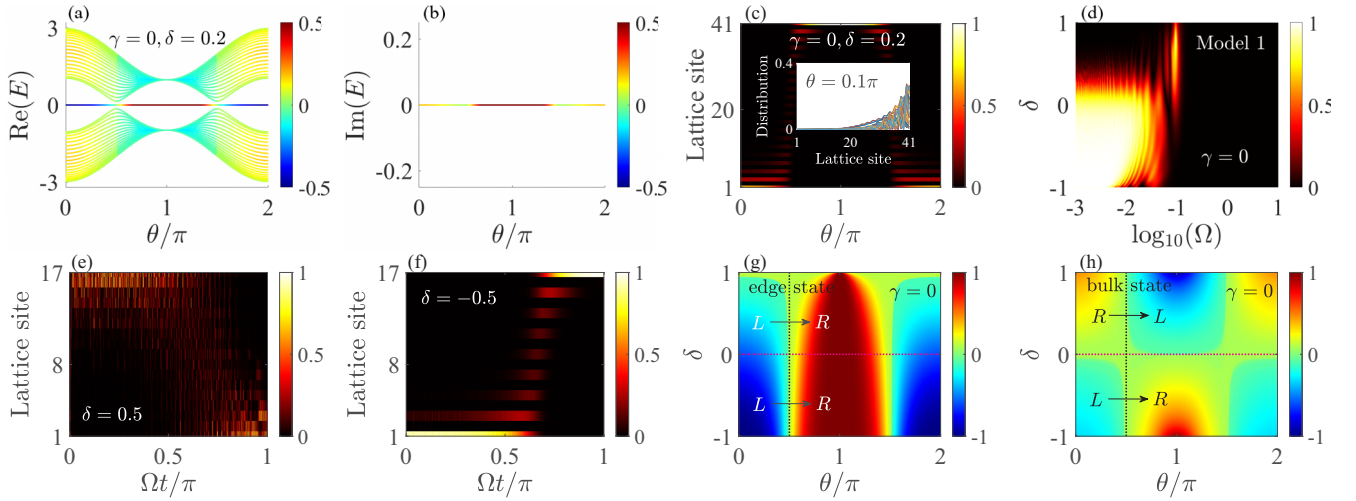

FIG. 3. Energy spectra, distributions of states, and fidelity for model 1 when $\gamma = 0$. (a) The real and (b) imaginary parts of the energy spectra when $\gamma = 0$ and $\delta = 0.2$. (c) The distributions of gap and bulk states. (d) The fidelity of topological excitation transmission versus varying speed Ω and amplitude of the imaginary potential γ. When $\Omega = 10^{-3}$, the evolutions of the excitation (e) with $\delta = 0.5$ and (f) with $\delta = -0.5$. The dIPRs versus parameters δ and θ for (g) edge state and (h) bulk states.

directional transmission toward the right edge. The reason can be attributed to the inconsistent localization directions of the gap state and bulk states caused by the parameters δ and θ. As shown in Fig. 3(a), when $\delta > 0$, the localization directions of the gap and bulk states are just opposite within $\theta \in [0, 2\pi]$; e.g., the gap state is localized around the left (right) edge when $\theta \in [0, 0.5\pi]$ ($\theta \in [0.5\pi, \pi]$), while the bulk states are mainly localized around the right (left) edge within the same range of the parameter θ.

To further clarify the different localization directions, the dIPR of the gap state versus the nonreciprocal parameter δ and periodic parameter θ is shown in Fig. 3(g). The results indicate that the nonreciprocal parameter δ cannot change the localization direction of the gap state within $\theta \in [0, \pi]$; i.e., the gap state is always localized at the left (right) edge when $\theta \in [0, 0.5\pi]$ ($\theta \in [0.5\pi, \pi]$). To estimate the effects of the parameter δ on the localization direction of the bulk states, we now define the directional mean inverse participation ratio (dMIPR) of all bulk states, i.e., $R_{\mathrm{dMIP}} = \frac{1}{L-1}\sum_k R_{\mathrm{dIP}}(\Psi_k)$. Here, $L-1$ denotes the number of bulk states. The dMIPR versus the parameters δ and θ is shown in Fig. 3(h). Obviously, the localization direction of the bulk states will be reversed for the cases with $\delta > 0$ and $\delta < 0$. More specifically, the bulk states are localized around the right (left) edge within $\theta \in [0, 0.5\pi]$ ($\theta \in [0.5\pi, \pi]$) when $\delta > 0$, while they are localized around the left (right) edge within $\theta \in [0, 0.5\pi]$ ($\theta \in [0.5\pi, \pi]$) when $\delta < 0$. Thus, compared with the localization direction of the gap state, the bulk states have the same localization direction only when $\delta < 0$, implying that the topological excitation transmission can be implemented only for negative δ.

Now we consider the joint effect of the purely imaginary potential and nonreciprocal intracell hopping, i.e., the case of $\gamma \neq 0$ and $\delta \neq 0$. The transmission efficiency versus the imaginary potential γ and nonreciprocal parameter δ is plotted in Fig. 4(a). The pattern of the fidelity is divided into two parts about the line $\gamma = 0$, in which the fidelity satisfies $F \sim 1$ when $\gamma > 0$ and changes as $F \sim 0$ when $\gamma < 0$. Note that the results within the parameter regions of $\gamma > 0$ and $\delta < 0$ are intuitive since the conditions of $\gamma > 0$ [see Fig. 2(d)] and $\delta < 0$ [see Fig. 3(d)] can both ensure the topological excitation transmission. Differently, we find that the topological excitation transmission can also be implemented within the parameter region of $\gamma > 0$ and $\delta > 0$ now. The different transmission behaviors corresponding to different γ and δ are shown in Figs. 4(b)–4(d), which show results consistent with the above analysis.

This phenomenon means that the positive purely imaginary potential can offset the adverse effect of the non-Hermitian skin effect when $\delta > 0$ [compared with Fig. 3(d)]. In other words, the effects of the imaginary potential on the topological excitation transmission are the dominant factor. Actually, this phenomenon can be comprehended via an effective

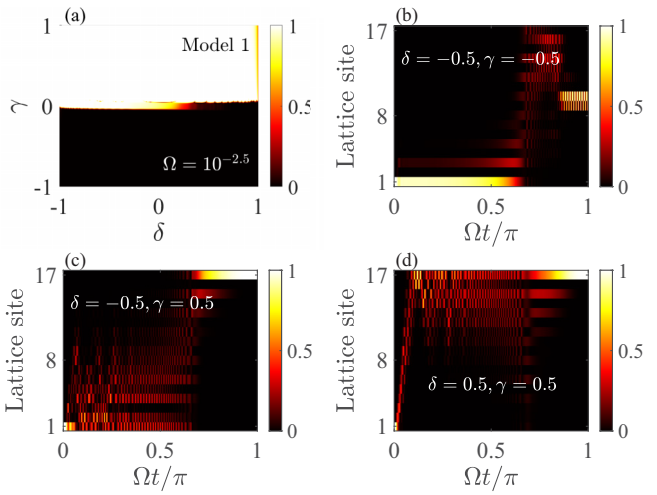

FIG. 4. Fidelity and evolutions of the excitation for model 1. (a) The fidelity of the topological excitation transmission versus the parameters δ and γ. (b)–(d) When $\Omega = 10^{-2.5}$, the evolutions of the excitation of different δ and γ.

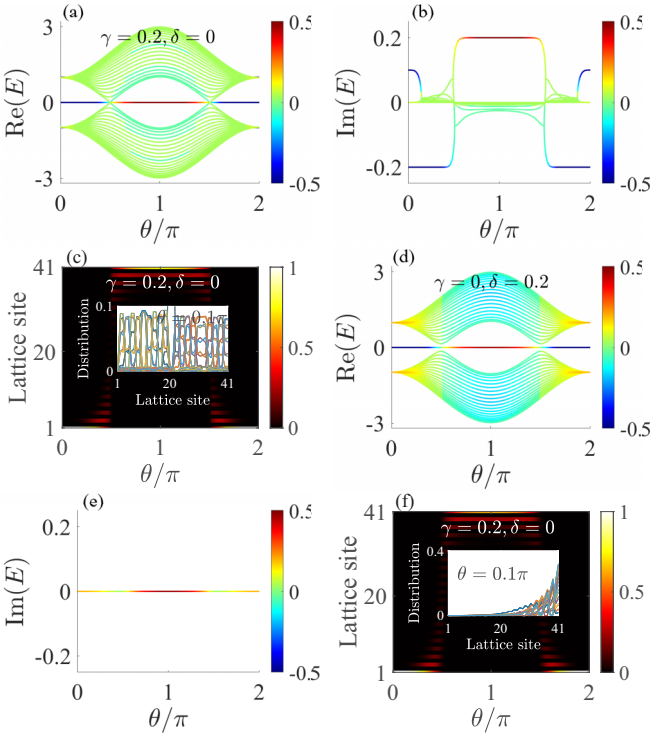

FIG. 5. Energy spectra and distributions of states for model 2. (a)–(c) Energy spectra and distributions of states when $\gamma = 0.2$ and $\delta = 0$. (d)–(f) Energy spectra and distributions of states when $\gamma = 0$ and $\delta = 0.2$.

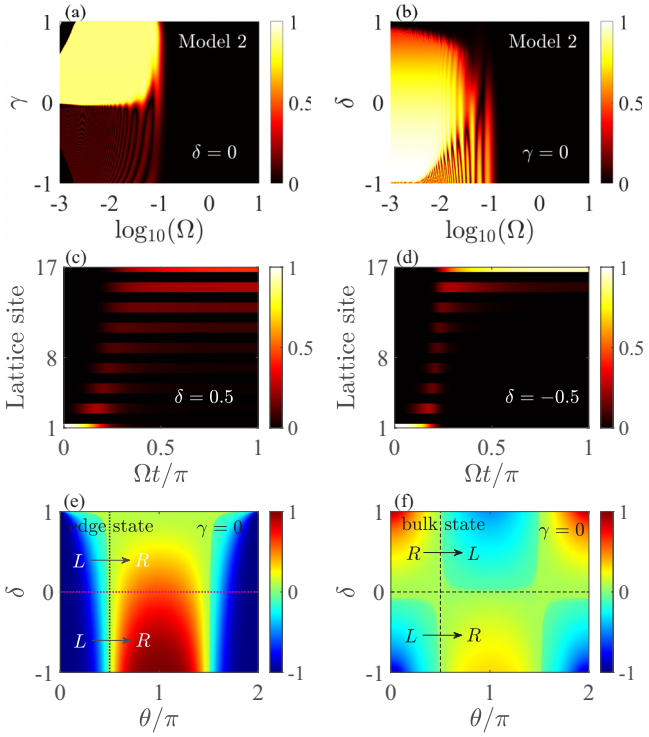

FIG. 6. Fidelity and evolutions of the excitation for model 2. The fidelity of the excitation transmission when (a) $\delta = 0$ and (b) $\gamma = 0$. When $\gamma = 0$ and $\Omega = 10^{-3}$, the evolutions of the excitation (c) with $\delta = 0.5$ and (d) with $\delta = -0.5$. The dIPRs versus parameters δ and θ for (g) the edge state and (h) bulk states.

lattice model by implementing the similarity transformation of the original model (see Appendix C). After the similarity transformation, the nonreciprocal intracell hopping can be replaced by an effective intracell hopping $J_e = \sqrt{J_{1,+}J_{1,-}} = \sqrt{1-(\delta\cos\theta)^2}$. Note that, for the parameters within $\delta \in [-1, 1]$ and $\theta \in [0, 2\pi]$, we have $1-(\delta\cos\theta)^2 \geqslant 0$, meaning that the amplitude of the effective intracell hopping corresponds to a real number. In this way, the present lattice model is equivalent to the lattice model mentioned in Ref. [72]; i.e., the SSH chain has only the purely imaginary on-site potential. Thus, the purely imaginary on-site potential determines the opening and closing of the topological excitation transmission.

D. Topological excitation transmission affected by nonreciprocal intercell hopping

We have investigated the effects of the imaginary on-site potential and nonreciprocal intracell hopping on the topological excitation transmission, i.e., the model shown in Fig. 1(a). Note that the right edge site in model 1 is coupled with the penultimate site via the reciprocal intercell hopping. Thus, it is an interesting question whether the different coupling configurations can affect the results mentioned above, e.g., the topological excitation transmission in the model shown in Fig. 1(b) (which we denote model 2). The energy spectra and distributions of states when $\delta = 0$ or $\gamma = 0$ for model 2 are plotted in Fig. 5. Figures 5(a) and 5(b) depict the real and imaginary parts of model 2 when $\delta = 0$. The results reveal the localized gap state and extended bulk states, which can be further verified via the distributions of states shown in Fig. 5(c). Note that, different from the case in Fig. 2(c), the present gap state cannot be localized at the last site completely. This means that the excitation initially prepared at the left edge may not be transmitted to the right edge completely. The energy spectra and distributions of states for model 2 when $\gamma = 0$ are shown in Figs. 5(d)–5(f). The results are similar to those in the case shown in Figs. 3(a)–3(c). Here, the main difference from the case in Fig 3(c) is the exchange localization locations of the gap state within $\theta \in [0, \pi]$.

The fidelities of the topological excitation transmission for model 2 when $\delta = 0$ or $\gamma = 0$ are shown in Figs. 6(a) and 6(b). We find that, when $\delta = 0$, the main parameter region for the topological excitation transmission with high fidelity is the same as in the case of model 1 [compare with Fig. 2(d)]. The difference is that the fidelity of the topological excitation transmission in model 2 cannot reach $F \sim 1$. The reason is that the gap state cannot be localized at the right edge completely when $\theta = \pi$, which means the excitation initially prepared at the left edge cannot be transmitted to the right edge completely. Meanwhile, when $\gamma = 0$, the main parameter region for the topological excitation transmission with fidelity $F \sim 1$ now becomes smaller than in the case shown in Fig. 3(d), meaning that the excitation initially prepared at the left edge can be transmitted to the right edge successfully only for the nonreciprocal parameter $\delta \sim -1$. The detailed processes of excitation transmission when $\delta = \pm 0.5$ are plotted in Figs. 6(c) and 6(d), which match the above analysis

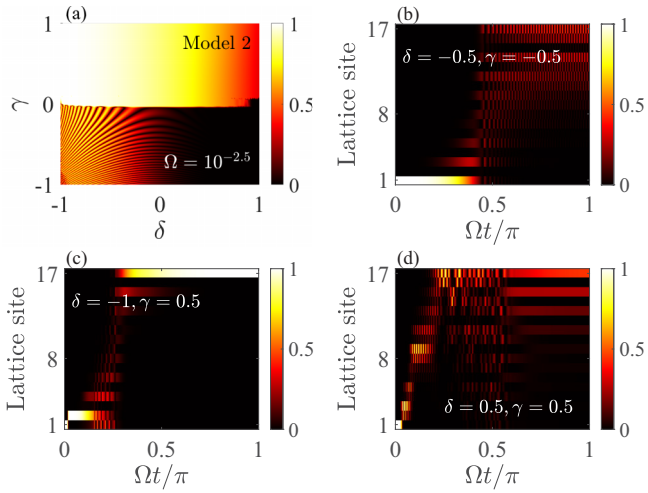

FIG. 7. Fidelity and evolutions of the excitation for model 2. (a) The fidelity of the topological excitation transmission versus the parameters δ and γ. (b)–(d) When $\Omega = 10^{-2.5}$, the evolutions of excitation for different δ and γ.

well. The localization properties of the gap and bulk states for model 2 when $\gamma = 0$ are shown in Figs. 6(e) and 6(f). The results reveal physics similar to that in the cases shown in Figs. 3(g) and 3(h).

The joint effect of the non-Hermitian parameters γ and δ on the topological excitation transmission in model 2 is plotted in Fig. 7(a). The results indicate that the excitation can be transmitted to the right edge successfully only when $\gamma > 0$ and $\delta \sim -1$, which is different from the case shown in Fig. 4(a). The reason can be explained as the dominant effect of the non-Hermitian skin effect in model 2 when $\delta \sim -1$. The evolutions of the excitation for different cases of parameters δ and γ are shown in Figs. 7(b)–7(d). We find that the excitation initially prepared at the left edge can be transmitted to the right edge successfully only when $\delta \sim -1$ and $\gamma > 0$ [Fig. 7(c)].

III. CONCLUSIONS

In conclusion, we have investigated the edge transmission behaviors of excitation in the SSH model with purely imaginary on-site potential and nonreciprocal NN hopping. We found that the purely imaginary on-site potential and nonreciprocal hopping can both affect the edge transmission of excitation. We demonstrated that, different from the effects of the purely imaginary on-site potential on the topological edge transmission, the localization direction of the non-Hermitian skin effect induced by nonreciprocal intracell hopping determines the opening or closing of the edge transmission; e.g., the edge transmission can be implemented only when the non-Hermitian skin effect has a localization direction consistent with the zero-energy gap state. We also investigated the joint effect of the purely imaginary on-site potential and nonreciprocal hopping on edge transmission, in which the different dominant roles of the purely imaginary on-site potential and nonreciprocal hopping were revealed. More specifically, the purely imaginary on-site potential determines the successful edge transmission when the nonreciprocal hopping is added to intracell hopping, while the nonreciprocal hopping added to intercell hopping is the dominant factor. Our investigations further supply the relevant contents of topological edge transmission in the non-Hermitian lattice system, which may promote applications of topological quantum information processing in open quantum system.

ACKNOWLEDGMENT

This work was supported by the National Natural Science Foundation of China under Grants No. 12304557, No. 12204404, and No. 12304472.

APPENDIX A: THE QUANTUM MAPPING OF NONRECIPROCAL HOPPING

Nonreciprocal hopping between two adjacent sites can be effectively implemented in a quantum system consisting of three modes [76,80,82]. As shown in Fig. 1(c), mode a and mode b can couple with each other directly with the coupling amplitude J_{ab}. Especially, mode a can also couple with mode b indirectly via an auxiliary mode c, in which the coupling amplitude between modes a (b) and c is $J_{ac}e^{i\phi}$ (J_{bc}). In this way, the three-mode system can be described by the following Hamiltonian:

$$H = \sum_{o=a,b,c} \omega_o o^\dagger o + (J_{ab}a^\dagger b + J_{ac}e^{-i\phi}a^\dagger c + J_{bc}b^\dagger c + \text{H.c.}). \tag{A1}$$

Here, ω_o denotes the free frequency of the three modes. If we set the three modes so that they have the same frequencies, i.e., $\omega_o = \omega$, the effective Hamiltonian under the rotating frame of free frequency ω can be written as

$$H' = (J_{ab}a^\dagger b + J_{ac}e^{-i\phi}a^\dagger c + J_{bc}b^\dagger c + \text{H.c.}). \tag{A2}$$

This can be understood as the fact that we reset the point of zero energy by removing the equal free energy of the three modes.

Under the regime of dissipation, the motion equations of operators for the three modes can be written as

$$\begin{aligned}
\dot{a} &= -\frac{\gamma_a}{2}a - iJ_{ac}e^{i\phi}c - iJb, \\
\dot{b} &= -\frac{\gamma_b}{2}b - iJa - iJ_{bc}c, \\
\dot{c} &= -\frac{\gamma_c}{2}c - iJ_{bc}b - iJ_{ac}e^{-i\phi}a,
\end{aligned} \tag{A3}$$

where γ_o represents the dissipation rate of the three modes. When the dissipation of mode c is large enough, mode c can be removed adiabatically by taking $\dot{c} = 0$, i.e.,

$$c = -i\frac{2}{\gamma_c}J_{bc}b - i\frac{2}{\gamma_c}J_{ac}e^{-i\phi}a. \tag{A4}$$

In this way, the motion equations of operators a and b now become

$$\begin{aligned}
\dot{a} &= -\frac{1}{2}\left(\gamma_a + \frac{4J_{ac}^2}{\gamma_c}\right)a - i\left(J - i\frac{2J_{ac}J_{bc}}{\gamma_c}e^{i\phi}\right)b, \\
\dot{b} &= -\frac{1}{2}\left(\gamma_b + \frac{2J_{bc}^2}{\gamma_c}\right)b - i\left(J - i\frac{2J_{ac}J_{bc}}{\gamma_c}e^{-i\phi}\right)a.
\end{aligned} \tag{A5}$$

If we further use the Heisenberg equation inversely, the effective Hamiltonian between modes a and b reads

$$H_{ab}^{\text{eff}} = (J - iJ'e^{-i\phi})b^{\dagger}a + (J - iJ'e^{i\phi})a^{\dagger}b. \tag{A6}$$

Here, we set $J' = \frac{2J_{ac}J_{bc}}{\gamma_c}$ for convenience. Obviously, when $\phi = 0.5\pi$, the nonreciprocal hopping between modes a and b can be implemented, i.e., $(J - J')b^{\dagger}a + (J + J')a^{\dagger}b$.

APPENDIX B: THE ADIABATIC THEORY AND SIZE EFFECT IN NON-HERMITIAN TOPOLOGICAL EXCITATION TRANSMISSIONS

The usual topological excitation transmission in the Hermitian system needs to satisfy the adiabatic condition to avoid the evolution evolving into the bulk around the gap closing point. Thus, the evolution speed Ω and minimal energy gap Δ_E usually need to satisfy $\sqrt{\Omega} < \Delta_E$ to ensure that the excitation is transmitted along the gap state [50]. Usually, the minimal energy gap Δ_E is exponentially decreased with increasing lattice size, causing the adiabatic condition to be tightened for a lattice with a large size. Different from the Hermitian lattice, the existence of imaginary energy in the non-Hermitian lattice may change the band structure and generate the effects on the dynamics of topological excitation transmission. Thus, the adiabatic condition and size effect in non-Hermitian topological excitation transmissions need to be considered.

Different from the Hermitian system, the significant difference in the non-Hermitian system is the existence of biorthonormal eigenstates

$$H|\psi_n\rangle = E_n|\psi_n\rangle, \quad H^{\dagger}|\phi_n\rangle = E_n^*|\phi_n\rangle, \tag{B1}$$

and $\langle\phi_k|\psi_n\rangle = \delta_{k,n}$. For the dynamical evolution of one state, $|\Phi(t)\rangle$, we can expand it in terms of the right eigenstate $|\psi_n\rangle$ with [83]

$$|\Phi(t)\rangle = \sum_n C_n(t)\exp\left[-i\int_0^t E_n(t')dt'\right]|\psi_n(t)\rangle. \tag{B2}$$

Note that the non-Hermitian system may cause the eigenvalue $E_n(t)$ to be complex, e.g., $E_n(t) = a_n(t) + ib_n(t)$. Thus, the relative probability amplitude in each eigenstate $|\psi_n\rangle$ satisfies $C_n(t)\exp[\int_0^t b_n(t')dt']$, which can be changed by varying the time. In this way, the evolution of state $|\Phi(t)\rangle$ cannot maintain itself, which may lead to the nonadiabatic effect.

Substituting Eq. (B2) into the Schrödinger equation $i\frac{\partial}{\partial t}|\Phi(t)\rangle = H(t)|\Phi(t)\rangle$ and multiplying the left eigenstate $\langle\phi_k(t)|$ [83], we have

$$\dot{C}_k(t) = -C_k(t)\langle\phi_k(t)|\dot{\psi}_k(t)\rangle - \sum_{k\neq n} C_n(t)\exp\left\{-i\int_0^t [E_n(t') - E_k(t')]dt'\right\}\langle\phi_k(t)|\dot{\psi}_n(t)\rangle. \tag{B3}$$

Obviously, if the eigenvalues are complex, e.g., $E_n(t) = a_n(t) + ib_n(t)$ and $E_k(t) = a_k(t) + ib_k(t)$, the amplitude in the term $\sum_{k\neq n} C_n(t)\exp\{-i\int_0^t [E_n(t') - E_k(t')]dt'\}\langle\phi_k(t)|\dot{\psi}_n(t)\rangle$ becomes $C_n(t)e^{\int_0^t [b_n(t') - b_k(t')]dt'}$, which can grow exponentially and cannot be neglected. Thus, if the non-Hermitian system corresponds to an imaginary spectrum, the adiabatic theorem cannot hold.

Differently, if the non-Hermitian system corresponds to a real spectrum, e.g., the case in Sec. II C, the second term on the right-hand side of Eq. (B3) can be safely removed by setting [83]

$$\left|\frac{\langle\phi_k(t)|\dot{\psi}_n(t)\rangle}{E_n - E_k}\right| \ll 1. \tag{B4}$$

After that, the probability amplitude satisfies $\dot{C}_k(t) \approx -C_k(t)\langle\phi_k(t)|\dot{\psi}_k(t)\rangle$, which has a form similar to the adiabatic parameter in the Hermitian system. In this way, the adiabatic theory is valid when the non-Hermitian system has the real spectrum. Interestingly, the non-Hermitian case of $\gamma \neq 0$ and $\delta = 0$ corresponds to an imaginary spectrum, while the case of $\gamma = 0$ and $\delta \neq 0$ just corresponds to a purely real spectrum. Thus, in the following, we will numerically show the nonadiabatic (adiabatic) evolution and size effect under these two non-Hermitian cases.

1. The non-Hermitian case with $\gamma \neq 0$ and $\delta = 0$

When $\gamma \neq 0$ and $\delta = 0$, the purely imaginary on-site potential leads to the appearance of an imaginary energy spectrum. The modulus of the energy spectrum when $\gamma = 0.2$ and $\delta = 0$ is shown in Fig. 8(a), and we define the minimal energy space as $\Delta|E|_{\text{min}}$. The minimal energy space $\Delta|E|_{\text{min}}$ versus the lattice size and the non-Hermitian parameter γ is shown in Fig. 8(b). We find that the minimal energy space approximately exhibits behavior similar to that in the Hermitian case; i.e., the minimal energy space decreases with increasing lattice size in a global view [see the inset in Fig. 8(b)]. However, the detailed behavior of the minimal energy space has a certain difference from the Hermitian case; i.e., the minimal energy space exhibits an oscillating behavior for a large lattice size. The oscillating behavior originates from the case in which the gap state enters into the bulk, as shown in Fig. 8(c). As we discussed above, the adiabatic theory is invalid when the non-Hermitian system has an imaginary energy spectrum.

To illustrate this clearly, we take lattice sizes $L = 5$ and $L = 61$ as examples. As shown in the inset of Fig. 8(b), when $L = 5$, the system has a large $\Delta|E|_{\text{min}}$, while the energy space $\Delta|E|_{\text{min}}$ is close to zero when $L = 61$.. According to the adiabatic theory in the Hermitian system, the narrowed energy space $\Delta|E|_{\text{min}}$ leads the evolution speed Ω to be slower, meaning that the transmission can be easily implemented in a lattice that is small in size. However, as shown in Fig. 8(d), we find that the evolution speed Ω has the same range with fidelity $F \sim 1$, indicating that the adiabatic theory in the present non-Hermitian system is invalid now. Especially for the case of $\Delta|E|_{\text{min}} \sim 0$ [e.g., $L = 61$ in Fig. 8(d)], if the adiabatic theory is valid, we need the evolution speed to be $\Omega \sim 0$. However, the results in Fig. 8(d) clearly show a successful transmission even when the evolution speed Ω is relatively large, which further reveals the invalid adiabatic theory in a non-Hermitian system with an imaginary spectrum. We stress that the above phenomenon is induced by the positive purely imaginary potential added to the right edge site, which enhances the probability distribution of the evolved state at the right edge site. Actually, the definition of fidelity $F = |\langle R|\Psi_f\rangle|$ can

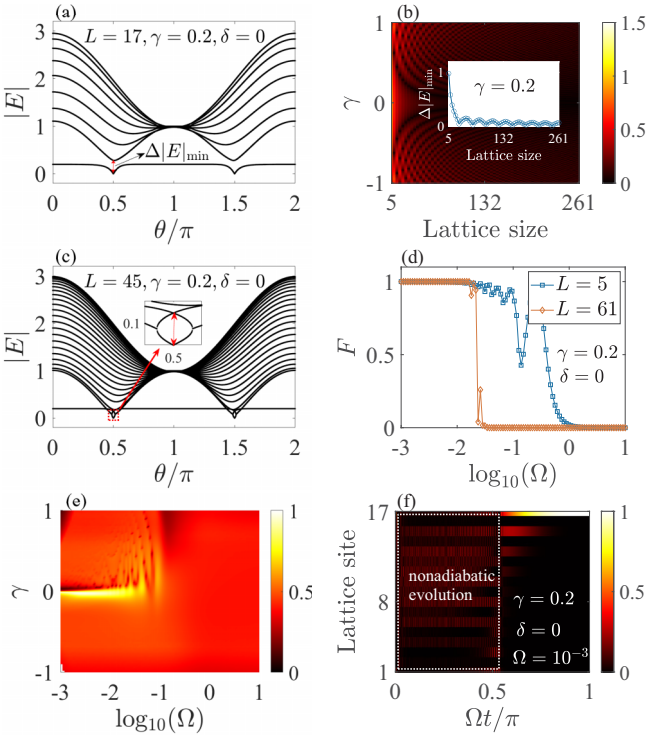

FIG. 8. Energy spectra, energy space, fidelity, average fidelity, and evolution in the non-Hermitian topological excitation transmissions. (a) Modulus of the energy spectrum when $\gamma = 0.2$, $\delta = 0$, and $L = 17$. (b) The minimal energy space versus the lattice size and γ when $\delta = 0$. (c) Modulus of the energy spectrum when $\gamma = 0.2$, $\delta = 0$, and $L = 45$. (d) The fidelity F versus the evolution speed for different lattice sizes when $\gamma = 0.2$ and $\delta = 0$. (e) The average fidelity $\bar{F}$ versus the evolution speed and non-Hermitian parameter γ when $\delta = 0$ and $L = 17$. (f) The evolution process of the non-Hermitian topological excitation transmission when $\gamma = 0.2$, $\delta = 0$, and $\Omega = 10^{-3}$.

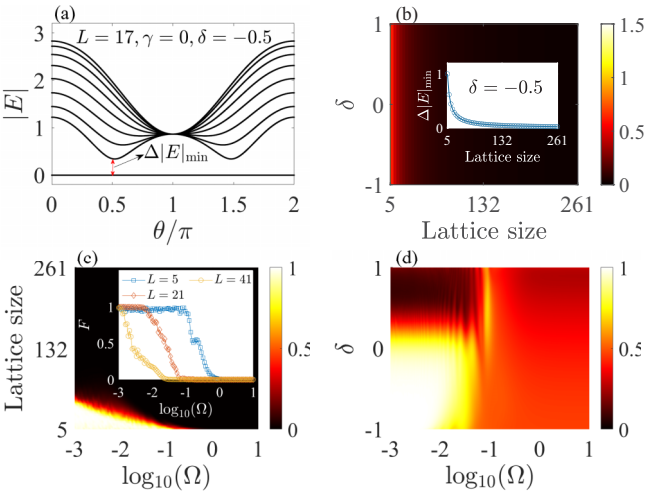

FIG. 9. Energy spectra, energy space, fidelity, and average fidelity in the non-Hermitian topological excitation transmissions. (a) Modulus of the energy spectrum when $\gamma = 0$, $\delta = -0.5$, and $L = 17$. (b) The minimal energy space versus the lattice size and δ when $\gamma = 0$. (c) The fidelity F versus the evolution speed and different lattice sizes when $\gamma = 0$ and $\delta = -0.5$. (d) The average fidelity $\bar{F}$ versus the evolution speed and nonreciprocal parameter δ when $L = 17$.

estimate only the final efficiency of the excitation at the right edge site, which cannot hold the process information of the evolution for the whole transmission process.

To evaluate the process information and show the nonadiabatic evolution visually, we now define the average fidelity of the non-Hermitian topological excitation transmission as

$$\bar{F} = 1/T \sum_{t=0}^{\pi/\Omega} F_t, \tag{B5}$$

where t is the discrete time originating from the numerical process, T is the total dimension of time t, and $F_t = |\langle\Psi_g(\theta_t)|\Psi_f(t)\rangle|$ is the fidelity between the evolved state and the boundary state solved by the energy eigenequation $H|\Psi_g(\theta_t)\rangle = E_g|\Psi_g(\theta_t)\rangle$ ($\theta_t = \Omega t$) at each time t. In this way, the average fidelity can be used to evaluate whether the excitation is transmitted along the boundary state. In other words, the average fidelity contains the complete information of the evolution process, while the fidelity F can estimate only whether the excitation is transmitted to the right edge at the final time. The average fidelity versus the evolution speed and non-Hermitian parameter γ is shown in Fig. 8(e). Obviously, the average fidelity $\bar{F}$ is large enough only when $\gamma \sim 0$, which means that this non-Hermitian topological excitation transmission indeed does not go along the boundary state. The nonadiabatic evolution can also be found from the process of excitation transmission, as shown in Fig. 8(f). The results clearly show that the evolution cannot match the distribution of the boundary state, implying that the transmission is, indeed, the nonadiabatic evolution (the evolution process generates the bulk diffusion).

2. The non-Hermitian case with $\gamma = 0$ and $\delta \neq 0$

Different from the case of $\gamma \neq 0$ and $\delta = 0$, the non-Hermitian case of $\gamma = 0$ and $\delta \neq 0$ corresponds to a real spectrum. As mentioned above, the appearance of the real spectrum ensures that the adiabatic theory is valid in such a non-Hermitian system. The modulus of the energy spectrum when $\gamma = 0$ and $\delta = -0.5$ is shown in Fig. 9(a), in which the spectrum exhibits consistency with the Hermitian lattice. Especially, we find the nonreciprocal parameter δ cannot affect the size effect of the minimal energy space; i.e., the minimal energy space $\Delta|E|_{\min}$ always decays exponentially with increasing lattice size for any nonreciprocal parameter δ [Fig. 9(b)]. To further estimate the adiabatic condition and the size effect when $\gamma = 0$ and $\delta \neq 0$, the fidelity F versus the evolution speed and lattice size is shown in Fig. 9(c). The results indicate that the fidelity exhibits the same size effect as the Hermitian case when $\delta < 0$ [see the inset of Fig. 9(c)]. The average fidelity $\bar{F}$ versus the evolution speed and the nonreciprocal parameter δ is shown in Fig. 9(d). The results clearly reveal that the region of $\bar{F} \sim 1$ is consistent with the fidelity F [compared with Fig. 3(d)], indicating that this topological excitation transmission indeed goes along the boundary state.

APPENDIX C: THE EFFECTIVE MODEL UNDER THE SIMILARITY TRANSFORMATION

The lattice model shown in Fig. 1(a), when $\gamma = 0$, can be written as

$$H_0 = \sum_{n=1}^{N}[J_{1,-}a_n^\dagger b_n + J_{1,+}b_n^\dagger a_n + J_2(a_{n+1}^\dagger b_n + \text{H.c.})], \tag{C1}$$

which corresponds to a SSH model having the nonreciprocal intracell hopping and reciprocal intercell hopping. For the Hamiltonian in Eq. (C1), we can perform a similarity transformation defined in real space, i.e.,

$$\bar{H}_0 = \mathcal{S}H_0\mathcal{S}^{-1}, \tag{C2}$$

with

$$\mathcal{S} = \text{diag}[1,\ r,\ r,\ r^2,\ r^2,\ \ldots,\ r^{N-1},\ r^N,\ r^N]. \tag{C3}$$

Here, $r = \sqrt{J_{1,-}/J_{1,+}}$ denotes the transformation factor, and N is the size of the unit cell. The Hamiltonian in Eq. (C1), under the similarity transformation, now becomes

$$\bar{H}_0 = \sum_{n=1}^{N}[J_e(a_n^\dagger b_n + b_n^\dagger a_n) + J_2(a_{n+1}^\dagger b_n + b_n^\dagger a_{n+1})], \tag{C4}$$

where $J_e = \sqrt{J_{1,+}J_{1,-}} = \sqrt{1-\delta^2\cos^2\theta}$ represents the effective intracell hopping after the similarity transformation. In this way, the original SSH model with nonreciprocal intracell hopping now becomes the SSH model with reciprocal intracell hopping J_e. Obviously, we have $J_e \in \text{Re}$ if the nonreciprocal parameter satisfies $|\delta| \leqslant 1$. In this way, the original lattice model becomes a Hermitian SSH model when $\gamma = 0$. Due to the fact that the similarity transformation cannot change the eigenvalues, the effective lattice model described in Eq. (C1) naturally has the same purely real spectrum [see Figs. 3(a) and 3(b)] as the Hermitian SSH model described in Eq. (C4).

Now, we consider the effects of purely imaginary on-site potential. Note that the above similarity transformation cannot change the diagonal terms of the matrix, leading the original Hamiltonian in Eq. (1) to become

$$H = \sum_{n=1}^{N/2}(-i\gamma a_n^\dagger a_n + i\gamma b_n^\dagger b_n) + \sum_{n=N/2+1}^{N}(-i\gamma b_n^\dagger b_n + i\gamma a_{n+1}^\dagger a_{n+1}) + \sum_{n=1}^{N}[J_e(a_n^\dagger b_n + b_n^\dagger a_n) + J_2(a_{n+1}^\dagger b_n + \text{H.c.})]. \tag{C5}$$

The above Hamiltonian obviously has the same form as the model in Ref. [72], which describes an odd-sized SSH chain with a purely imaginary potential. Thus, the positive purely imaginary on-site potential determines the opening of the topological excitation transmission [see Fig. 4(a)].

[1] M. Saffman, T. G. Walker, and K. Mølmer, Quantum information with Rydberg atoms, Rev. Mod. Phys. **82**, 2313 (2010).

[2] D. Suter and G. A. Álvarez, Colloquium: Protecting quantum information against environmental noise, Rev. Mod. Phys. **88**, 041001 (2016).

[3] A. Galindo and M. A. Martín-Delgado, Information and computation: Classical and quantum aspects, Rev. Mod. Phys. **74**, 347 (2002).

[4] L.-M. Duan and C. Monroe, Colloquium: Quantum networks with trapped ions, Rev. Mod. Phys. **82**, 1209 (2010).

[5] C. Monroe, Quantum information processing with atoms and photons, Nature (London) **416**, 238 (2002).

[6] C. H. Bennett and D. P. DiVincenzo, Quantum information and computation, Nature (London) **404**, 247 (2000).

[7] H. Jeong, M. S. Kim, and J. Lee, Quantum-information processing for a coherent superposition state via a mixedentangled coherent channel, Phys. Rev. A **64**, 052308 (2001).

[8] J. S. Neergaard-Nielsen, B. M. Nielsen, C. Hettich, K. Mølmer, and E. S. Polzik, Generation of a superposition of odd photon number states for quantum information networks, Phys. Rev. Lett. **97**, 083604 (2006).

[9] A. Feix, M. Araújo, and Č. Brukner, Quantum superposition of the order of parties as a communication resource, Phys. Rev. A **92**, 052326 (2015).

[10] M. C. de Oliveira and W. J. Munro, Quantum computation with mesoscopic superposition states, Phys. Rev. A **61**, 042309 (2000).

[11] S. B. Zheng, Quantum-information processing and multiatom-entanglement engineering with a thermal cavity, Phys. Rev. A **66**, 060303(R) (2002).

[12] S. B. Zheng and G.-C. Guo, Efficient scheme for two-atom entanglement and quantum information processing in cavity QED, Phys. Rev. Lett. **85**, 2392 (2000).

[13] D. S. Naik, C. G. Peterson, A. G. White, A. J. Berglund, and P. G. Kwiat, Entangled state quantum cryptography: Eavesdropping on the Ekert protocol, Phys. Rev. Lett. **84**, 4733 (2000).

[14] T. Jennewein, C. Simon, G. Weihs, H. Weinfurter, and A. Zeilinger, Quantum cryptography with entangled photons, Phys. Rev. Lett. **84**, 4729 (2000).

[15] J. Yin *et al.*, Entanglement-based secure quantum cryptography over 1,120 kilometres, Nature (London) **582**, 501 (2020).

[16] J. I. Cirac, P. Zoller, H. J. Kimble, and H. Mabuchi, Quantum state transfer and entanglement distribution among distant nodes in a quantum network, Phys. Rev. Lett. **78**, 3221 (1997).

[17] S. Bose, Quantum communication through an unmodulated spin chain, Phys. Rev. Lett. **91**, 207901 (2003).

[18] M. Christandl, N. Datta, A. Ekert, and A. J. Landahl, Perfect state transfer in quantum spin networks, Phys. Rev. Lett. **92**, 187902 (2004).

[19] G. M. Nikolopoulos and I. Jex, *Quantum State Transfer and Network Engineering, Quantum Science and Technology* (Springer, Heidelberg, 2013).

[20] K. Eckert, O. Romero-Isart, and A. Sanpera, Efficient quantum state transfer in spin chains via adiabatic passage, New J. Phys. **9**, 155 (2007).

[21] M. Christandl, N. Datta, T. C. Dorlas, A. Ekert, A. Kay, and A. J. Landahl, Perfect transfer of arbitrary states in quantum spin networks, Phys. Rev. A **71**, 032312 (2005).

[22] Y. L. Zhou, Y. M. Wang, L. M. Liang, and C. Z. Li, Quantum state transfer between distant nodes of a quantum network via adiabatic passage, Phys. Rev. A **79**, 044304 (2009).

[23] M. Lubasch, V. Murg, U. Schneider, J. I. Cirac, and M. C. Bañuls, Adiabatic preparation of a Heisenberg antiferromagnet using an optical superlattice, Phys. Rev. Lett. **107**, 165301 (2011).

[24] U. Farooq, A. Bayat, S. Mancini, and S. Bose, Adiabatic many-body state preparation and information transfer in quantum dot arrays, Phys. Rev. B **91**, 134303 (2015).

[25] M. Röntgen, C. V. Morfonios, I. Brouzos, F. K. Diakonos, and P. Schmelcher, Quantum network transfer and storage with compact localized states induced by local symmetries, Phys. Rev. Lett. **123**, 080504 (2019).

[26] D. Matsukevich and A. Kuzmich, Quantum state transfer between matter and light, Science **306**, 663 (2004).

[27] Y. Guo, D. Dong, and C. C. Shu, Optimal and robust control of quantum state transfer by shaping the spectral phase of ultrafast laser pulses, Phys. Chem. Chem. Phys. **20**, 9498 (2018).

[28] Y. Qi, C. C. Shu, D. Dong, I. R. Petersen, K. Jacobs, and S. Gong, Fast quantum state transfer in hybrid quantum dot-metal nanoparticle systems by shaping ultrafast laser pulses, J. Phys. D **52**, 425101 (2019).

[29] Y. H. Chen, Q. C. Wu, B.-H. Huang, J. Song, and Y. Xia, Arbitrary quantum state engineering in three-state systems via counterdiabatic driving, Sci. Rep. **6**, 38484 (2016).

[30] S. Longhi, Adiabatic quantum state transfer in tight-binding chains using periodic driving fields, Europhys. Lett. **107**, 50003 (2014).

[31] F. Beaudoin, A. Blais, and W. Coish, Hamiltonian engineering for robust quantum state transfer and qubit readout in cavity QED, New J. Phys. **19**, 023041 (2017).

[32] Y. H. Kang, Y. H. Chen, Q. C. Wu, B. H. Huang, Y. Xia, and J. Song, Reverse engineering of a Hamiltonian by designing the evolution operators, Sci. Rep. **6**, 30151 (2016).

[33] M. H. Yung and S. Bose, Perfect state transfer, effective gates, and entanglement generation in engineered bosonic and fermionic networks, Phys. Rev. A **71**, 032310 (2005).

[34] A. Jayashankar and P. Mandayam, Pretty good state transfer via adaptive quantum error correction, Phys. Rev. A **98**, 052309 (2018).

[35] A. Kay, Quantum error correction for state transfer in noisy spin chains, Phys. Rev. A **93**, 042320 (2016).

[36] G. Tajimi and N. Yamamoto, Dynamical Gaussian state transfer with quantum-error-correcting architecture, Phys. Rev. A **85**, 022303 (2012).

[37] Y. E. Kraus, Y. Lahini, Z. Ringel, M. Verbin, and O. Zilberberg, Topological states and adiabatic pumping in quasicrystals, Phys. Rev. Lett. **109**, 106402 (2012).

[38] M. Verbin, O. Zilberberg, Y. Lahini, Y. E. Kraus, and Y. Silberberg, Topological pumping over a photonic Fibonacci quasicrystal, Phys. Rev. B **91**, 064201 (2015).

[39] N. Y. Yao, C. R. Laumann, A. V. Gorshkov, H. Weimer, L. Jiang, J. I. Cirac, P. Zoller, and M. D. Lukin, Topologically protected quantum state transfer in a chiral spin liquid, Nat. Commun. **4**, 1585 (2013).

[40] M. Bello, C. E. Creffield, and G. Platero, Long-range doublon transfer in a dimer chain induced by topology and ac fields, Sci. Rep. **6**, 22562 (2016).

[41] P. Gao and J. Christensen, Topological sound pumping of zero-dimensional bound states, Adv. Quantum Technol. **3**, 2000065 (2020).

[42] L. Qi, N. Han, S. Hu, and A. L. He, Engineering the unidirectional topological excitation transmission and topological diode in the Rice-Mele model, Phys. Rev. A **108**, 032402 (2023).

[43] J. Alicea, Y. Oreg, G. Refael, F. Von Oppen, and M. Fisher, Non-Abelian statistics and topological quantum information processing in 1D wire networks, Nat. Phys. **7**, 412 (2011).

[44] M. Z. Hasan and C. L. Kane, Colloquium: Topological insulators, Rev. Mod. Phys. **82**, 3045 (2010).

[45] X. L. Qi and S. C. Zhang, Topological insulators and superconductors, Rev. Mod. Phys. **83**, 1057 (2011).

[46] C. K. Chiu, J. C. Y. Teo, A. P. Schnyder, and S. Ryu, Classification of topological quantum matter with symmetries, Rev. Mod. Phys. **88**, 035005 (2016).

[47] A. Bansil, H. Lin, and T. Das, Colloquium: Topological band theory, Rev. Mod. Phys. **88**, 021004 (2016).

[48] C. Dlaska, B. Vermersch, and P. Zoller, Robust quantum state transfer via topologically protected edge channels in dipolar arrays, Quantum Sci. Technol. **2**, 015001 (2017).

[49] N. Lang and H. P. Büchler, Topological networks for quantum communication between distant qubits, npj Quantum Inf. **3**, 47 (2017).

[50] F. Mei, G. Chen, L. Tian, S. L. Zhu, and S. Jia, Robust quantum state transfer via topological edge states in superconducting qubit chains, Phys. Rev. A **98**, 012331 (2018).

[51] J. L. Tambasco, G. Corrielli, R. J. Chapman, A. Crespi, O. Zilberberg, R. Osellame, and A. Peruzzo, Quantum interference of topological states of light, Sci. Adv. **4**, eaat3187 (2018).

[52] L. Qi, G. L. Wang, S. Liu, S. Zhang, and H.-F. Wang, Controllable photonic and phononic topological state transfers in a small optomechanical lattice, Opt. Lett. **45**, 2018 (2020).

[53] M. I. N. Rosa, R. K. Pal, J. R. F. Arruda, and M. Ruzzene, Edge states and topological pumping in spatially modulated elastic lattices, Phys. Rev. Lett. **123**, 034301 (2019).

[54] Y. X. Shen, L. S. Zeng, Z. G. Geng, D. G. Zhao, Y. G. Peng, and X. F. Zhu, Acoustic adiabatic propagation based on topological pumping in a coupled multicavity chain lattice, Phys. Rev. Appl. **14**, 014043 (2020).

[55] L. Qi, G. L. Wang, S. Liu, S. Zhang, and H. F. Wang, Engineering the topological state transfer and topological beam splitter in an even-sized Su-Schrieffer-Heeger chain, Phys. Rev. A **102**, 022404 (2020).

[56] M. Makwana, R. Craster, and S. Guenneau, Topological beam-splitting in photonic crystals, Opt. Express **27**, 16088 (2019).

[57] X. S. Wang, Y. Su, and X. R. Wang, Topologically protected unidirectional edge spin waves and beam splitter, Phys. Rev. B **95**, 014435 (2017).

[58] L. Qi, Y. Yan, Y. Xing, X. D. Zhao, S. Liu, W. X. Cui, X. Han, S. Zhang, and H. F. Wang, Topological router induced via long-range hopping in a Su-Schrieffer-Heeger chain, Phys. Rev. Res. **3**, 023037 (2021).

[59] L. N. Zheng, X. Yi, and H. F. Wang, Engineering a phase-robust topological router in a dimerized superconducting-circuit lattice

with long-range hopping and chiral symmetry, Phys. Rev. Appl. **18**, 054037 (2022).

[60] S. Longhi, G. L. Giorgi, and R. Zambrini, Landau–Zener topological quantum state transfer, Adv. Quantum Technol. **2**, 1800090 (2019).

[61] S. Longhi, Topological pumping of edge states via adiabatic passage, Phys. Rev. B **99**, 155150 (2019).

[62] F. M. D'Angelis, F. A. Pinheiro, D. Guéry-Odelin, S. Longhi, and F. Impens, Fast and robust quantum state transfer in a topological Su-Schrieffer-Heeger chain with next-to-nearest-neighbor interactions, Phys. Rev. Res. **2**, 033475 (2020).

[63] N. E. Palaiodimopoulos, I. Brouzos, F. K. Diakonos, and G. Theocharis, Fast and robust quantum state transfer via a topological chain, Phys. Rev. A **103**, 052409 (2021).

[64] S. Malzard, C. Poli, and H. Schomerus, Topologically protected defect states in open photonic systems with non-Hermitian charge-conjugation and parity-time symmetry, Phys. Rev. Lett. **115**, 200402 (2015).

[65] H. C. Wu, L. Jin, and Z. Song, Topology of an anti-parity-time symmetric non-Hermitian Su-Schrieffer-Heeger model, Phys. Rev. B **103**, 235110 (2021).

[66] R. Okugawa and T. Yokoyama, Topological exceptional surfaces in non-Hermitian systems with parity-time and parity-particle-hole symmetries, Phys. Rev. B **99**, 041202(R) (2019).

[67] K. Kawabata, Y. Ashida, H. Katsura, and M. Ueda, Parity-time-symmetric topological superconductor, Phys. Rev. B **98**, 085116 (2018).

[68] L. Xiao *et al.*, Observation of topological edge states in parity–time-symmetric quantum walks, Nat. Phys. **13**, 1117 (2017).

[69] H. Shackleton and M. S. Scheurer, Protection of parity-time symmetry in topological many-body systems: Non-Hermitian toric code and fracton models, Phys. Rev. Res. **2**, 033022 (2020).

[70] T. Chen, B. Wang, and X. Zhang, Characterization of topological phases and selection of topological interface modes in the parity-time-symmetric quantum walk, Phys. Rev. A **97**, 052117 (2018).

[71] N. Okuma and Y. O. Nakagawa, Nonnormal Hamiltonian dynamics in quantum systems and its realization on quantum computers, Phys. Rev. B **105**, 054304 (2022).

[72] L. Qi, N. Han, S. Liu, H. F. Wang, and A. L. He, Controllable excitation transmission and topological switch based on an imaginary topological channel in a non-Hermitian Su-Schrieffer-Heeger chain, Phys. Rev. A **107**, 062214 (2023).

[73] S. Yao and Z. Wang, Edge states and topological invariants of non-Hermitian systems, Phys. Rev. Lett. **121**, 086803 (2018).

[74] F. Song, S. Yao, and Z. Wang, Non-Hermitian skin effect and chiral damping in open quantum systems, Phys. Rev. Lett. **123**, 170401 (2019).

[75] S. Longhi, Probing non-Hermitian skin effect and non-Bloch phase transitions, Phys. Rev. Res. **1**, 023013 (2019).

[76] Q. Liang, D. Xie, Z. Dong, H. Li, H. Li, B. Gadway, W. Yi, and B. Yan, Dynamic signatures of non-Hermitian skin effect and topology in ultracold atoms, Phys. Rev. Lett. **129**, 070401 (2022).

[77] K. Kawabata, M. Sato, and K. Shiozaki, Higher-order non-Hermitian skin effect, Phys. Rev. B **102**, 205118 (2020).

[78] N. Okuma, K. Kawabata, K. Shiozaki, and M. Sato, Topological origin of non-Hermitian skin effects, Phys. Rev. Lett. **124**, 086801 (2020).

[79] S. Longhi, D. Gatti, and G. D. Valle, Robust light transport in non-Hermitian photonic lattices, Sci. Rep. **5**, 13376 (2015).

[80] L. Du, Y. Zhang, and J. H. Wu, Controllable unidirectional transport and light trapping using a one-dimensional lattice with non-Hermitian coupling, Sci. Rep. **10**, 1113 (2020).

[81] Q. B. Zeng and R. Lü, Real spectra and phase transition of skin effect in nonreciprocal systems, Phys. Rev. B **105**, 245407 (2022).

[82] X. W. Xu, Y. Li, B. Li, H. Jing, and A. X. Chen, Nonreciprocity via nonlinearity and synthetic magnetism, Phys. Rev. Appl. **13**, 044070 (2020).

[83] Q. Zhang and B. Wu, Non-Hermitian quantum systems and their geometric phases, Phys. Rev. A **99**, 032121 (2019).